An Efficient Electromagnetic-Physics-Based Numerical Technique for Modeling and Optimization of High-Frequency Multifinger Transistors

Yasser A. Hussein, *Member, IEEE*, Samir M. El-Ghazaly, *Fellow, IEEE*, and Stephen M. Goodnick, *Senior Member, IEEE*

***Abstract*—We present a fast wavelet-based time-domain modeling technique to study the effect of electromagnetic (EM)-wave propagation on the performance of high-power and high-frequency multifinger transistors. The proposed approach solves the active device model that combines the transport physics, and Maxwell's equations on nonuniform self-adaptive grids, obtained by applying wavelet transforms followed by hard thresholding. This allows forming fine and coarse grids in the locations where variable solutions change rapidly and slowly, respectively. A CPU time reduction of 75% is achieved compared to a uniform-grid case, while maintaining the same degree of accuracy. After validation, the potential of the developed technique is demonstrated by EM-physical modeling of multifinger transistors. Different numerical examples are presented, showing that accurate modeling of high-frequency devices should incorporate the effect of EM-wave propagation and electron-wave interactions within and around the device. Moreover, high-frequency advantages of multifinger transistors over single-finger transistors are underlined through numerical examples. To our knowledge, this is the first time in the literature a fully numerical EM-physics-based simulator for accurate modeling of high-frequency multifinger transistors is introduced and implemented.**

***Index Terms*—Full hydrodynamic model, global modeling, Maxwell's equations, multifinger transistors, multiresolution time domain (MRTD), semiconductor simulation, wavelets.**

I. Introduction

MULTIFINGER transistors have proven better performance over conventional transistors, especially at very high frequency [1]–[11]. However, until now, modeling of such devices did not account for electromagnetic (EM)-wave propagation effects, as well as electron-wave interactions using a fully numerical simulator. Accordingly, it is indispensable to present analysis of multifinger transistors based on a coupled EM-physics-based simulator. The possibility of achieving this type of modeling is addressed by global circuit modeling, which has been demonstrated in [12]–[17].

Global modeling is a tremendous task that involves advanced numerical techniques and different algorithms. As a result, it is computationally expensive [17]. Therefore, there is an imperative need to develop a new approach to reduce the simulation time, while maintaining the same degree of accuracy presented by global-modeling techniques. One approach is to adaptively refine grids in locations where the unknown variables vary rapidly. Such a technique is called multiresolution time domain (MRTD), and a very attractive way to implement it is to use wavelets [18], [19].

The MRTD approach has been successfully applied to finite-difference time-domain (FDTD) simulations of passive structures [20]–[31]. However, for the active devices, which are characterized by a set of coupled and highly nonlinear partial differential equations (PDEs), applying the same approach would become quite time consuming [32]. Several different approaches for solving PDEs using wavelets have been considered. It has been observed by several authors that nonlinear operators such as multiplication are too computationally expensive when conducted directly on a wavelet basis. One of the approaches for solving PDEs is the interpolating-wavelets technique presented in [33], in which the nonlinearities are dealt with using the so-called sparse point representation (SPR). Interpolating wavelets have been successfully applied to the simple drift-diffusion active-device model [34]–[36]. Being primarily developed for long-gate devices, the drift-diffusion model leads to inaccurate estimations of device internal distributions and microwave characteristics for submicrometer devices [37]. It is worth mentioning that, in [33], the author proposed a new technique to solve simple forms of hyperbolic PDEs using an interpolating-wavelet scheme. These PDEs can represent Maxwell's equations or the simple drift-diffusion model, but not the complete hydrodynamic model. Thus, a new approach to apply wavelets to the hydrodynamic model PDEs is needed, along with extending it to Maxwell's equations, for accurate modeling of submicrometer devices, while achieving a CPU time reduction.

In this paper, a unified approach to apply wavelets to the full hydrodynamic model and Maxwell's equations is developed.

Manuscript received April 17, 2003. This work was supported by the U.S. Army Research Office under Contract DAAD-19-99-1-0194.

Y. A. Hussein was with the Department of Electrical Engineering, Arizona State University, Tempe, AZ 85287 USA. He is now with the Stanford Linear Accelerator Center, Stanford University, Menlo Park, CA 94025 USA (e-mail: yasser@SLAC.Stanford.EDU).

S. M. El-Ghazaly is with the Department of Electrical and Computer Engineering, University of Tennessee, Knoxville, TN 37996 USA (e-mail: El-ghazaly@utk.edu).

S. M. Goodnick is with the Department of Electrical Engineering, College of Engineering and Applied Science, Arizona State University, Tempe, AZ 85287-5706 USA (e-mail: Stephen.Goodnick@asu.edu).

Digital Object Identifier 10.1109/TMTT.2003.820160

The main idea is to take snapshots of the solution during the simulation, and apply wavelet transform to the current solution to obtain the coefficients of the details. The coefficients of the details are then normalized, and a threshold is applied to obtain a nonuniform grid. Two independent grid-updating criteria are developed for the active and passive parts of the problem. Moreover, a threshold formula that is dependent on the variable solution at any given time has been developed and verified. In addition, a full-wave global-modeling simulator is developed to study the EM-wave propagation effect on high-power and frequency multifinger transistors. A comprehensive set of results is included along with illustrative comparison graphs.

This paper is organized as follows. Section II briefly reviews the theory of MRTD. Problem description is given in Section III. Full descriptions of the proposed algorithm along with illustrative graphs are provided in Section IV. Technique validation is presented in Section V. Error and stability analysis are discussed in Section VI. Microwave characteristics of high-frequency transistors are provided in Section VII, and results of EM physical modeling of multifinger transistors are presented in Section VIII. Finally, conclusions are provided in Section IX.

II. Fundamentals of MRTD

The construction of biorthogonal wavelet bases relies on the notation of multiresolution analysis [38]. This notation gives a formal description of the intuitive idea that every signal can be constructed by a successive refinement by iteratively adding *details* to an *approximation*. The coefficients of the approximations are given by

$$a_x[n,m] = \int_{-\infty}^{+\infty} x(t)\varphi_{nm}(t)\,dt \tag{1}$$

where $\varphi_{nm}(t)$ is the family of dilates and translates of the scaling function formed as

$$\varphi_{nm}(t) = 2^{m/2}\varphi(2^m t - n). \tag{2}$$

On the other hand, (3) gives the coefficients of the details as follows:

$$d_x[n,m] = \int_{-\infty}^{+\infty} x(t)\psi_{nm}(t)\,dt \tag{3}$$

where $\psi_{nm}(t)$ is the family of dilates and translates of the wavelet function defined as

$$\left\{\psi_{nm}(t) = 2^{m/2}\psi\big(2^m t - n\big); n,m \in Z\right\}. \tag{4}$$

While some wavelets such as Daubechies are asymmetrical [38], it is possible to create symmetric wavelets with compact support by using two sets of wavelets: one to compose the signal and the other to construct it. Such wavelets are called *biorthogonal* [39].

III. Problem Description

The transistor model used in this study is a three-dimensional (3-D) large-signal EM-physical model. The active device model is based on the moments of the Boltzmann's transport equation (BTE) obtained by integrating over the momentum space. The integration results in a strongly coupled highly nonlinear set of PDEs called the conservation equations. These equations provide a time-dependent self-consistent solution for carrier density, carrier energy, and carrier momentum, which are given as follows.

- *Current continuity*

$$\frac{\partial n}{\partial t} + \nabla\cdot(n\upsilon) = 0. \tag{5}$$

- *Energy conservation*

$$\frac{\partial(n\varepsilon)}{\partial t} + qn\upsilon\cdot\boldsymbol{E} + \nabla\cdot(n\upsilon(\varepsilon + K_B T)) = -\frac{n(\varepsilon-\varepsilon_0)}{\tau_\varepsilon(\varepsilon)}. \tag{6}$$

- *x-momentum conservation*

$$\frac{\partial(np_x)}{\partial t} + qnE_x + \frac{\partial}{\partial x}(np_x\upsilon_x + nK_B T) = -\frac{n(p_x - p_0)}{\tau_m(\varepsilon)}. \tag{7}$$

In the above equations, n is the electron concentration, υ is the electron velocity, $\boldsymbol{E}$ is the electric field, ε is the electron energy, ε_0 is the equilibrium thermal energy, and p is the electron momentum. The energy and momentum relaxation times are given by τ_ε and τ_m, respectively. Similar expression can be obtained for the y-direction momentum. The three conservation equations are solved in conjunction with Maxwell's equations

$$\nabla\times\boldsymbol{E} = -\frac{\partial\boldsymbol{B}}{\partial t} \tag{8}$$

$$\nabla\times\boldsymbol{H} = \frac{\partial\boldsymbol{D}}{\partial t} + \boldsymbol{J} \tag{9}$$

where $\boldsymbol{E}$ is the electric field, $\boldsymbol{H}$ is the magnetic field, $\boldsymbol{D}$ is the electric flux density, and $\boldsymbol{B}$ is the magnetic flux density. The fields in Maxwell's equations are updated using the current density $\boldsymbol{J}$ estimated by (10) as follows:

$$\boldsymbol{J}(t) = -qn\upsilon(t). \tag{10}$$

The low field mobility is given by the empirical relation [40]

$$\mu_0 = \frac{8000}{1 + (N_d\cdot 10^{-17})^{0.5}}\ \text{cm}^2/\text{V}\cdot\text{s}. \tag{11}$$

The above model accurately describes all the nonstationary transport effects by incorporating energy dependence into all the transport parameters such as effective mass and relaxation times, along with including EM-wave effects. Fig. 1 shows the cross section of the simulated structure with parameters summarized in Table I.

IV. Proposed Algorithm

Fig. 2 shows the flowchart of the proposed algorithm. A uniform grid is defined at the beginning of the simulation. Equations (5)–(7) are then solved in the sequence shown by

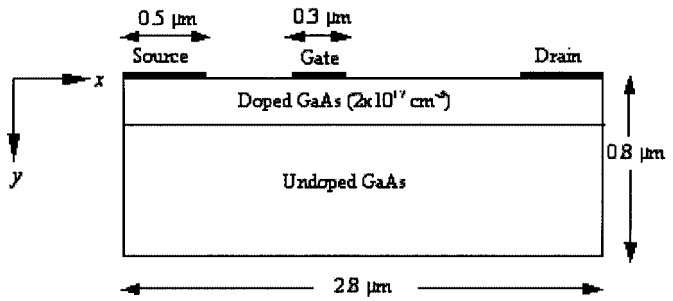

Fig. 1. Cross section of the simulated transistor.

TABLE I
TRANSISTOR PARAMETERS USED IN THE SIMULATION

Drain and source contacts	0.5 μm
Gate-source separation	0.5 μm
Gate-drain separation	1.0 μm
Device thickness	0.8 μm
Device length	2.8 μm
Gate length	0.3 μm
Device Width	250 μm
Active layer thickness	0.2 μm
Active layer doping	$2\text{x}10^{17}$ cm^{-3}
Schottky barrier height	0.8 V
DC gate-source voltage	-0.5 V
DC drain-source voltage	3.0 V

the flowchart to update the grid of the different variables at the new iteration with the following criterion:

$$\frac{\left|x^{l}_{\max,\min} - x^{c}_{\max,\min}\right|}{\left|x^{l}_{\max,\min}\right|} \geq \delta_{\text{Hydro}}. \tag{12}$$

The updating criterion checks if the solution of the variable x has changed by δ_{Hydro} since the last iteration using wavelet transform. The subscripts c and l designate quantities defined in the current time and last time where wavelet transform is performed, respectively. The subscript "max, min" indicates that the maximum and minimum of the variable x are checked with (12) at the same time. It is significant to note here that boundary grid points are not included for the maximum or minimum checking. The value of δ_{Hydro} used in the simulation is 0.1. If (12) is satisfied, wavelet transform is performed on the current variable solution followed by hard thresholding to obtain a new nonuniform grid for the variable x. Biorthogonal wavelets are used with notation BIO3.1 to point out three vanishing moments for the mother wavelet and only one vanishing moment for the scaling function. The nonuniform grids of the different variables are then combined into only one nonuniform grid for the next iteration. The above steps are repeated until the stopping criterion is satisfied.

It should be noted that magnitude ranges of the variables used in the simulations vary dramatically. For instance, carrier density per cm^{-3} is on the order of 10^{17}, while energy expressed in electronvolts is on the order of 0.5. Accordingly, the threshold

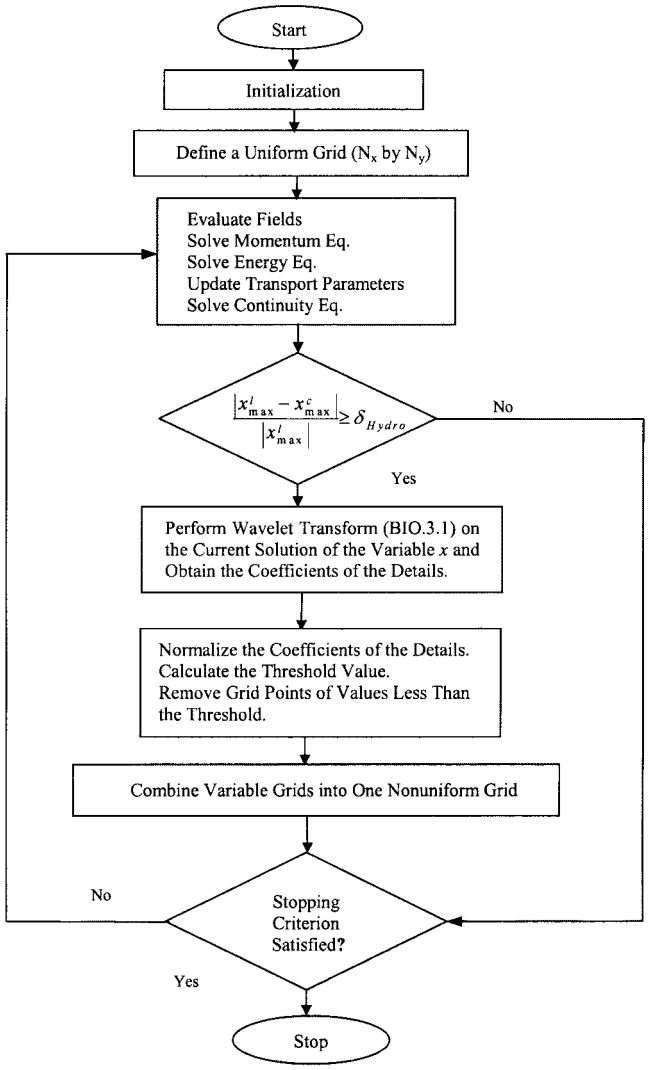

Fig. 2. Generic flowchart of the proposed algorithm.

value should be dependent on the variable solution at any given iteration. The proposed threshold formula is given as

$$T = \frac{T_0}{N}\left[\sqrt{\sum_{i=1}^{N} d_i^2}\right]. \tag{13}$$

In this equation, T_0 is the initial threshold value, d_i's are the coefficients of the details, and N is the number of grid points in the x- or y-direction. Hence, the value of the threshold depends mainly on the variable solution at any given time rather than being fixed. The values of T_0 used in the simulation are 0.001, 0.01, and 0.05, respectively.

It is significant to note that the proposed algorithm is carefully developed such that it is general and device independent. This includes the threshold value given by (13). Considering this equation, it is clear that it has no device-dependent parameters. Furthermore, the different values of T_0 are used only to investigate the tradeoffs between CPU time and accuracy, which is a general approach provided by papers introducing similar

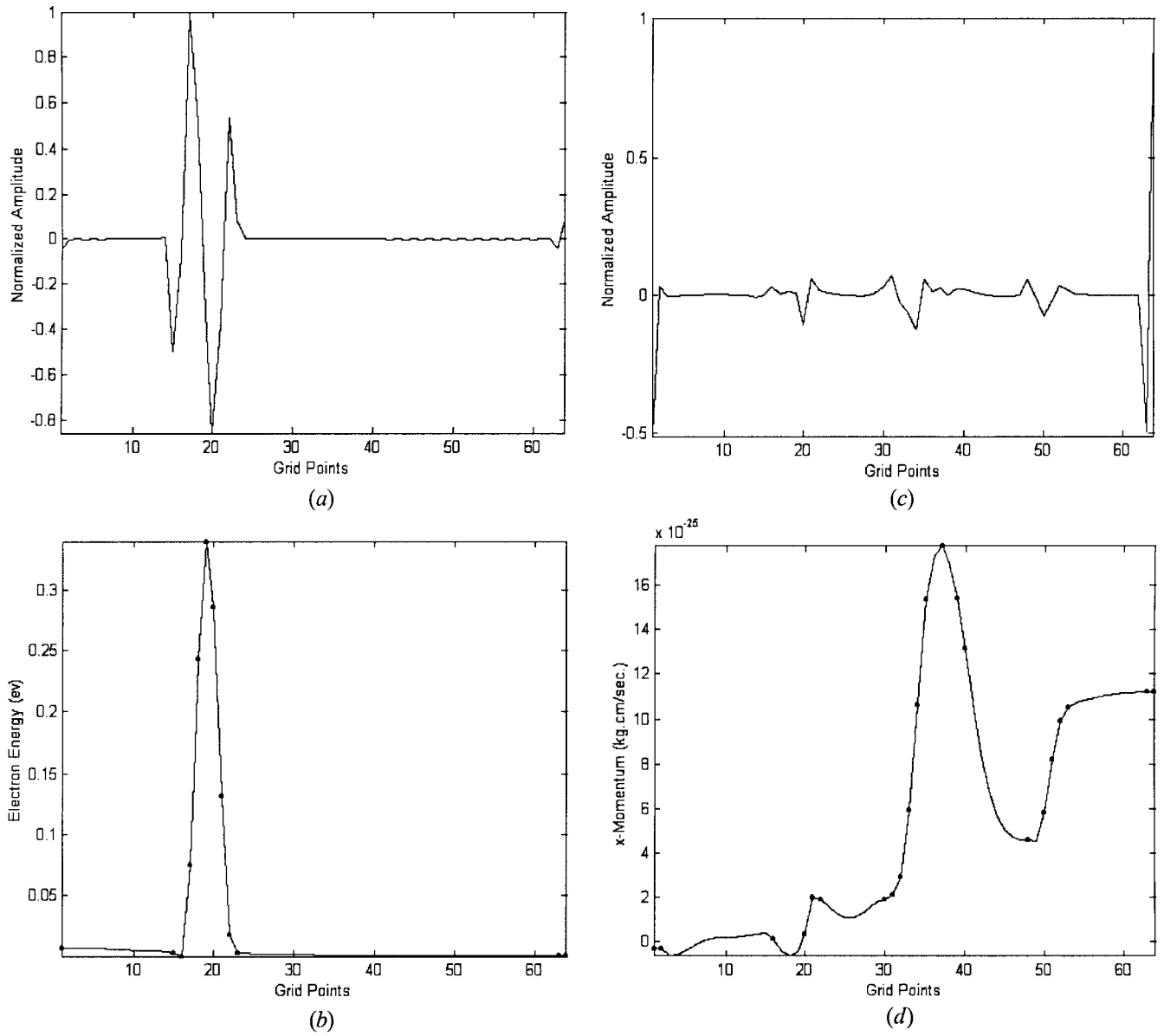

Fig. 3. (a) Normalized details coefficients for the electron energy at a certain longitudinal cross section. (b) Grid points marked on the actual curve for the electron energy at the same longitudinal cross section. (c) Normalized details coefficients for the x-momentum at a certain longitudinal cross section. (d) Grid points marked on the actual curve for the x-momentum at the same longitudinal cross section.

threshold-controlled wavelet-based techniques, e.g., in [21] and [35].

In this paper, a new technique to conceive the nonuniform grids using wavelets has been developed. The main idea is to apply wavelet transform to the variable solution at any given time to obtain the coefficients of the details, which are then normalized to its maximum. Only grid points where the value of the normalized coefficients of the details larger than the threshold value given by (13) are included. Fig. 3 exemplifies how the proposed algorithm obtains the nonuniform grid using longitudinal compression only. For instance, Fig. 3(a) shows the normalized amplitude of the coefficients of the details for the electron energy, while, Fig. 3(b) marks the grid points remaining after thresholding the normalized coefficients of the details using (13). It should be observed that the proposed technique accurately removes grid points in the locations where variable solutions change very slowly.

The overall grid obtained needs further processing in order to define a finite-difference (FD) scheme on it. The simplest way to achieve that is to have the same number of grid points for the parallel cross sections, while the number of grid points in the longitudinal cross sections and transverse cross sections need not be the same. Following the above procedure, it was found that boundary conditions implementation, including ohmic and Schottky contacts, does not need special treatment. They can be treated similar to the standard FD scheme. The only issue the algorithm needs to keep track of is identifying the new boundaries of the metallic contacts for each new grid, which is straightforward.

Table II shows the evolution of the nonuniform grids. It can be observed that the number of grid points for the overall grid increases as time advances. The reason is that, at the beginning of the simulation, the solution is not completely formed yet and, as time marches, more grid points are needed to incorporate the

TABLE II
GRID ADAPTABILITY OF THE DIFFERENT VARIABLES FOR $T_0 = 1\%$

Variable	Unknowns Remaining After Transverse Compression (%)	Unknowns Remaining After Longitudinal Compression (%)	Total Unknowns Remaining (%)
	Time Iteration # 120		
Potential	5.69	7.74	0.63
Carrier Density	6.54	14.92	2.64
Energy	39.65	17.63	8.54
x-Momentum	43.39	16.06	9.18
y-Momentum	16.11	17.53	3.78
All Variables	65.14	22.36	14.43
	Time Iteration # 250		
Potential	5.88	8.59	0.76
Carrier Density	13.69	16.70	5.18
Energy	39.21	23.00	12.26
x-Momentum	43.65	19.09	10.64
y-Momentum	20.02	19.46	7.95
All Variables	61.94	28.93	20.58
	Time Iteration # 480		
Potential	6.27	9.23	0.90
Carrier Density	21.51	17.16	7.71
Energy	43.99	28.88	15.72
x-Momentum	38.57	23.44	12.72
y-Momentum	26.20	26.76	13.53
All Variables	58.84	36.25	25.05
	Time Iteration # 590		
Potential	6.04	9.64	0.93
Carrier Density	29.88	18.24	10.61
Energy	48.85	31.88	18.43
x-Momentum	41.91	29.08	16.21
y-Momentum	32.91	37.04	20.36
All Variables	62.36	44.73	31.74
	Time Iteration # 730		
Potential	7.01	11.13	1.15
Carrier Density	34.08	16.55	8.42
Energy	39.77	35.64	18.43
x-Momentum	41.91	27.98	13.32
y-Momentum	51.46	34.84	25.00
All Variables	62.84	58.96	36.43

changes in the solution. Furthermore, the different variable grids should not be updated at the same rate. For instance, it is apparent that the potential needs not to be updated at the same rate as the other variables. Notice that Table II is used for illustration purposes to demonstrate the way the different variable grids change. In the actual simulation, the potential grid is updated a few times at the beginning of the simulation, and then it remains unchanged.

Now we turn our attention to Maxwell's equations. The passive part of the field-effect transistor (FET) represents a coplanar structure in which a 3-D FDTD code is developed to solve for the electric and magnetic fields. The current density estimated from the active device conversation equations is used to update the fields in Maxwell's equations.

It is importance to state that the same approach developed to obtain the nonuniform grid for the variables of the conversation equations is applied to Maxwell's equations as well. However, a different updating mechanism should be developed to keep track of the wave propagation within the structure. The following is the algorithm developed for the grid updating of FDTD simulations.

Step 1) Construct a 3-D matrix M that has only 0's and 1's based on whether or not we have a nonzero solution of the field at this location. For example, "1" is assigned if a nonzero field solution exists, and "0" is assigned elsewhere.

Step 2) Estimate the value of δ_{FDTD} (FDTD grid-updating factor) as

$$\delta_{\mathrm{FDTD}} = \frac{\sum_{i,j,k}(M_{\mathrm{new}} \oplus M_{\mathrm{old}})_{i,j,k}}{N_{xd}N_{yd}N_{zd}} \tag{14}$$

where M_{new} and M_{old} are the matrices constructed using step one for the current and old solutions of the fields, respectively. N_{xd}, N_{yd}, and N_{zd} are the number of grid points in the x-, y-, and z-directions, respectively.

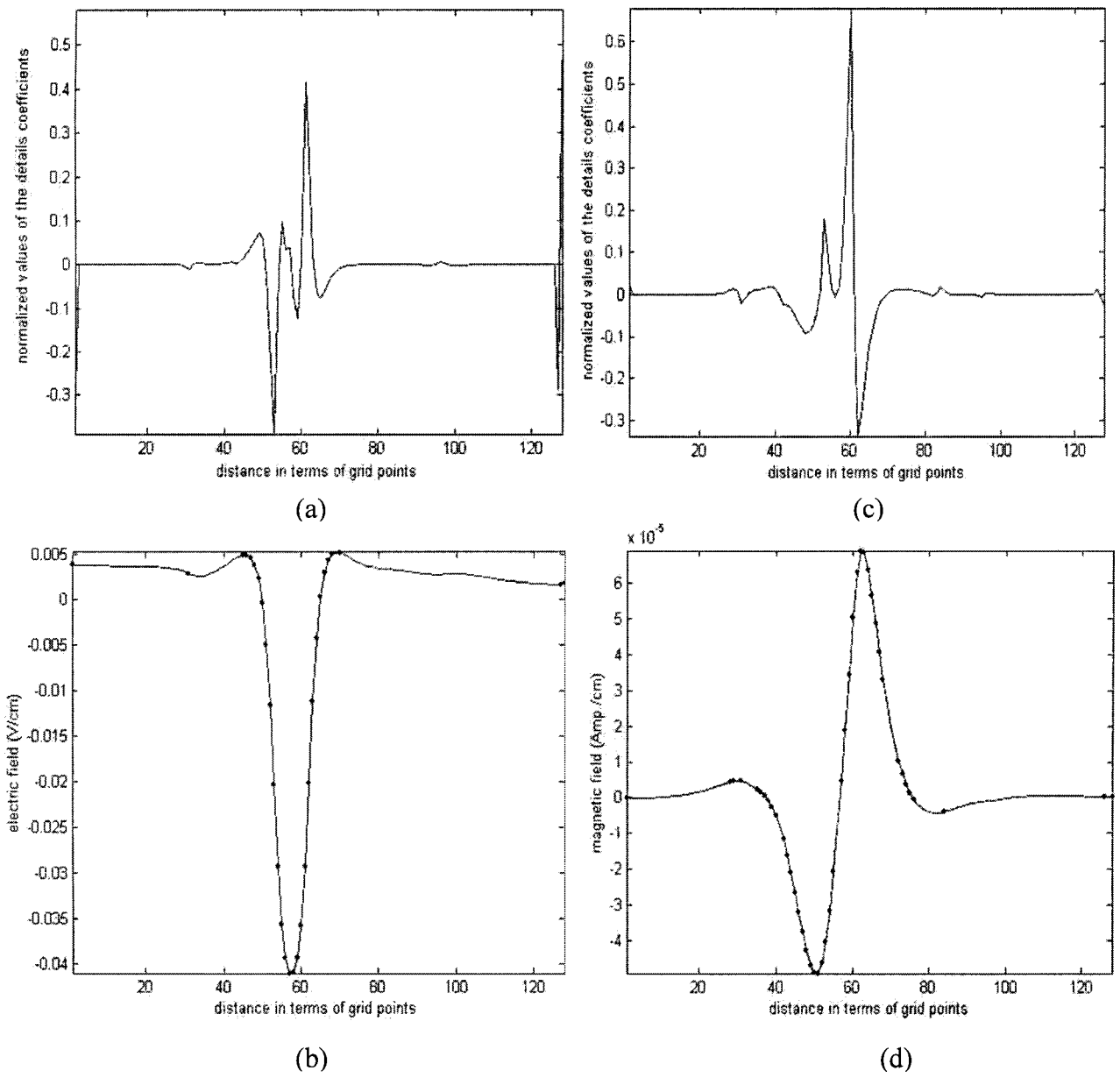

Fig. 4. Demonstration of the procedure employed to obtain the nonuniform grid for the y-direction electric and magnetic fields for FDTD simulations.

Step 3) Check δ_{FDTD}'s value against a predefined value, e.g., 5%.

Step 4) If satisfied, move the grid to $z = z + dz$, where dz is proportional to δ_{FDTD}.

Step 5) $t = t + dt$.

Fig. 4 illustrates examples of how the nonuniform grids are obtained for the magnetic and electric fields at a specific cross section for FDTD simulations. For instance, Fig. 4(a) shows the normalized amplitude of the coefficients of the details for the electric field, while Fig. 4(b) marks the grid points remaining after thresholding the normalized coefficients of the details using (13). It is observed that the proposed technique accurately removes the grid points in locations where variable solutions change very slowly. This would have an effect of reducing the CPU time by removing the redundant grid points introduced by the original formulation. The overall grid of the electric field is achieved by obtaining two separate grids for the transverse and longitudinal compressions, respectively. The two grids are then combined using logical "AND" to conceive the overall grid for the electric field at any given time. It is worth mentioning here that the excitation wave exists at the source plan at all times, and the technique proposed here is generic and can also be applied to a short pulse propagating in the computational domain.

V. Technique Validation

A. Hydrodynamic Model Simulation Results

The approach presented in this paper is general and can be applied to any unipolar transistor. To demonstrate the potential of this approach, it is applied to an idealized FET structure, which is discretized by a mesh of $64\Delta x$ by $64\Delta y$ with $\Delta t = 0.001$ ps. Forward Euler is adopted as an explicit

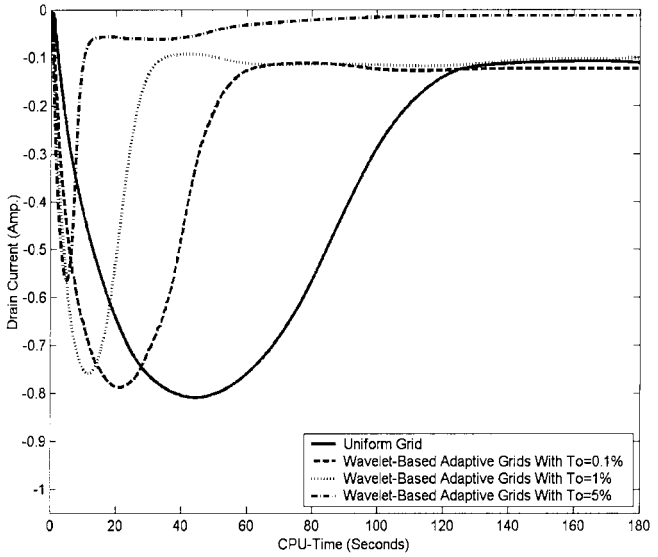

Fig. 5. DC drain-current convergence curves for the uniform grid and the proposed wavelet-based nonuniform grids for different initial threshold values.

FD method. In addition, upwinding is employed to have a stable FD scheme. The space step sizes are adjusted to satisfy Debye length, while the time-step value Δt is chosen to satisfy the Courant–Friedrichs–Lewy (CFL) condition. First, dc simulations are performed following the flowchart given by Fig. 2, and the current density is calculated using (10). DC excitation is performed by forcing the potential to be equal to the applied voltages to the electrodes (i.e., Dirichlet boundary conditions).

It is important to note that a suitable approach to investigate the capabilities of the proposed technique is to compare it to the uniform-grid algorithm. In this case, the new simulator will be accurately evaluated. Since both algorithms, the wavelet-based and uniform one, will run on the same computer. In addition, both algorithms will have the same discritization schemes and the exact semiconductor parameters.

Fig. 5 shows the drain current convergence curves versus the CPU time in seconds for the cases of the uniform grid and the proposed wavelet-based adaptive grids with different initial threshold values. Fig. 5 demonstrates that using the proposed wavelet-based grids approach reduces the CPU time dramatically. For instance, there is a reduction of approximately 75% in CPU time over the uniform grid case for the initial threshold value of 1%, while the dc drain current error is within 1%. In addition, increasing the initial threshold beyond a certain value has a negative effect on the accuracy of the final results. This is apparent for T_0 equals to 5%, where there is no agreement between the results achieved using the uniform grid case and the wavelet-based nonuniform grids. The reason is that using large values of T_0 implies that more grid points are removed, including important grid points that will have a negative effect on the final result. On the other hand, using a very small threshold values implies redundant grid points. In summary, there should be an optimal value of T_0 such that both the CPU time and error are minimized. In this study, T_0 of 1% is suggested to have a considerable reduction in CPU time, while keeping the error within an acceptable range.

TABLE III
EFFECT OF THE THRESHOLD VALUE ON ERROR AND CPU TIME FOR FDTD SIMULATIONS

T_0	*CPU-Time (Seconds)*	*Error*	
		2-norm	*∞-norm*
0.0 (Uniform Grid)	744.90		
0.1%	300.17	0.0873%	8.80%
1.0%	205.92	0.0871%	8.75%
5.0%	155.10	0.0778%	7.69%
10.0%	111.05	0.0473%	3.66%

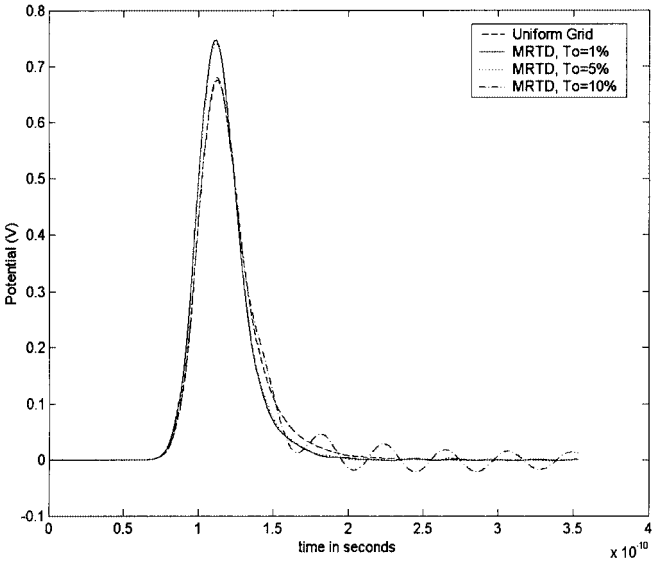

Fig. 6. Potential of the gate at a specific cross section versus time for the uniform grid case and the proposed MRTD algorithm with different values of T_0.

The specific problem presented in this paper is provided only to validate the new algorithm, and to emphasize that practical problems have solutions that change very rapidly only in specific domains. Accordingly, an algorithm could be implemented to exploit that by solving the equations on multiresolution-nonuniform grids, obtained using wavelets. Obviously, the amount of CPU time reduction depends on the problem under consideration. More or less reduction should be achieved for other types of problems depending on the sharpness and distribution of fields in the computational domain.

B. FDTD Simulation Results

A 3-D Yee-based FDTD code is developed, with the proposed algorithm employed. A Guassian excitation pulse is applied to evaluate the algorithm over a wide range of frequencies. Table III shows that, as threshold value increases, CPU time and error introduced decreases as well. It is noteworthy to point out that using an initial threshold value equals to 10% seems to reduce error along with the CPU time. However, considering Fig. 6, one should conclude that using T_0 equals to 10% introduces dispersion, which is a serious type of error. Accordingly, an initial threshold value of 5% is recommended in terms of both CPU time and error for FDTD simulations. It is important to emphasize that the passive and active parts of the problem have different optimal threshold values. This is

expected since the variables in the conservations equations are highly nonlinear compared to the fields obtained when solving Maxwell's equations. More details describing the research work presented in this paper can be found in [41]–[43].

VI. Scheme Error and Stability Analysis

It is important to mention here that the simulation and physical times are completely separate entities. The simulation time required to model a specific physical process should vary depending on the technique implemented in the simulation.

The purpose of this section is to demonstrate that the mechanism by which error is introduced when employing the proposed wavelet-based technique is different than of the uniform-grid case. The local truncation error for the uniform grid case is dependent, in general, on the mesh spacing (Δx and Δy) and the time step used Δt. On the other hand, the local truncation error for the wavelet-based nonuniform grids approach depends on how accurately the important grid points are reserved, as well as the time step used. This suggests that the local truncation errors, due to spatial discritization, for the uniform grid case and the wavelet-based nonuniform grids are different. The local truncation error accumulates from iteration to iteration. The total truncation or discritization error is thus dependent on the number of iterations used (space and time iterations combined). Accordingly, one can conclude that the total error introduced by the wavelet-based technique due to the local discritization errors accumulating during the simulation may or may not be larger than that of the uniform grid case, at least for the two cases of $T_0 = 0.1\%$ and $T_0 = 1\%$. The reason is the number of iterations required to reach the steady-state solution for the uniform grid case is much larger than that of the proposed algorithm. In summary, the total error introduced depends on the local truncation error along with the number of iterations required to reach the final solution. This explains the results in this paper's comparison figures, where it would be difficult to draw a precise conclusion of which technique is more accurate. This is because, for each case or curve, the number of iterations required to obtain the steady-state solution and local discritization errors are different. The problem of identifying the most accurate solution becomes even more difficult since we are dealing with a highly nonlinear problem.

It is significant to call attention to the fact that the proposed algorithm does not have any stability constraints if Δt is chosen to satisfy the CFL condition at the beginning of the simulation. The reason is, as the simulation progresses, the spatial distances employed become even larger than the ones introduced at the beginning. This represents an extra benefit of using the proposed algorithm because it does not need any time-step Δt change while the simulation is in progress.

VII. Microwave Characteristics of High-Frequency Transistors

To study the characteristics of transistors at high frequency, a time-domain Guassian signal is applied between the source and gate electrodes. The input and output time-domain signals are observed at different points along the width of the device. The characteristics of the device are then estimated. For example, the propagation constant γ can be evaluated as

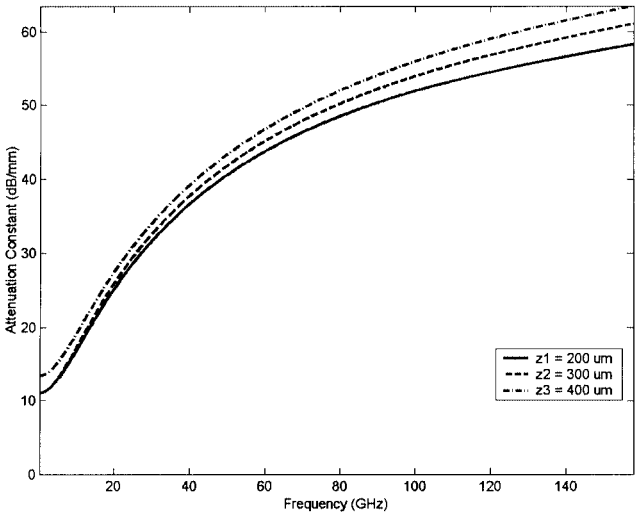

Fig. 7. Attenuation constant as a function of frequency at different points along the device width for the gate electrode.

$$\gamma = \frac{1}{l} \log_e \left\{ \frac{F(\omega, z+l)}{F(\omega, z)} \right\} \tag{15}$$

where $F(\omega, z)$ is the Fourier transform of the time-domain signal. The attenuation and propagation constants are evaluated as the real and imaginary parts of γ, respectively. Fig. 7 shows the attenuation constant as a function of frequency at different points along the device width. Considering Fig. 7, it should be noticed that the attenuation constant increases with frequency, as well as from point to point along the device width.

The phase velocity $v_{\rm ph}$ and effective dielectric constant ε_r can be estimated using (16) and (17), respectively,

$$v_{\rm ph} = \frac{\omega}{\beta} \tag{16}$$

$$\varepsilon_r = \frac{\beta^2 c^2}{(2\pi f)^2} \tag{17}$$

where β is the propagation constant, c is the free-space wave velocity, and ω is the frequency in radians per second. Figs. 8 and 9 show the effective dielectric constant and phase velocity versus frequency at different points along the device width, respectively. The results shown in Figs. 8 and 9 are mainly due to the change of the distribution of the electric field as a function of frequency and distance. These results are distinctive to high-frequency devices only, which could be exploited by employing optimized microwave structures such as multifinger transistors. The results presented in this section coincide, conceptually, with those presented in [44], i.e., the effective dielectric constant decreases and increases with frequency for the gate and drain modes, respectively. It is worth mentioning that these results are contrary to those obtained for passive structures, where the effective dielectric constant should increase with frequency.

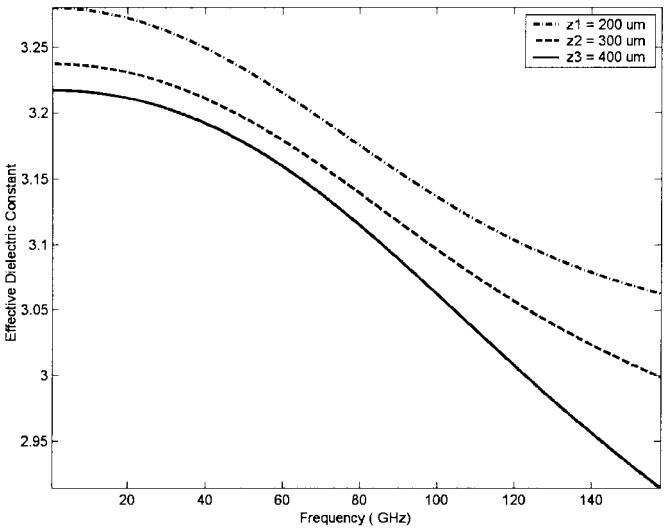

Fig. 8. Effective dielectric constant as a function of frequency at different points along the device width for the gate electrode.

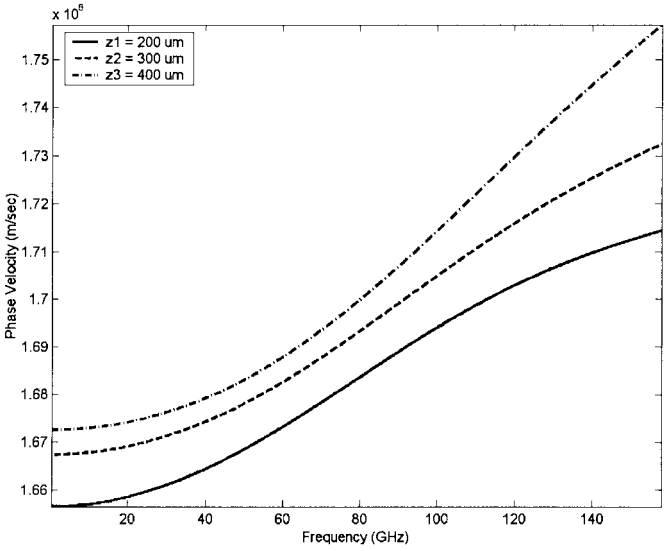

Fig. 9. Phase velocity as a function of frequency at different points along the device width for the gate mode.

VIII. EM-Wave Effects on High-Frequency Multifinger Transistors

A. EM-Wave Propagation Effects and Electron-Wave Interactions

In this section, a full-wave physical simulator is developed to model two closely packed millimeter-wave transistors. Fig. 10 gives a 3-D view of the simulated transistors. The simulated devices are biased to $V_{\rm ds} = 3.0$ V and $V_{\rm gs} = -0.1$ V. The gate length for the transistors is set to 0.2 μm. The dc distributions are obtained by solving the active device model with Poisson's equation. A sinusoidal signal is employed in the ac simulations with a peak value of 100 mV and frequency of 80 GHz, respectively. The two transistors shown in Fig. 10 are identical. First, full-wave simulations are carried out for one transistor only, and the results are depicted in Fig. 11. Considering this figure, one should observe the variations of the output voltage with distance along the device width. The reasons are due to the nonlinear

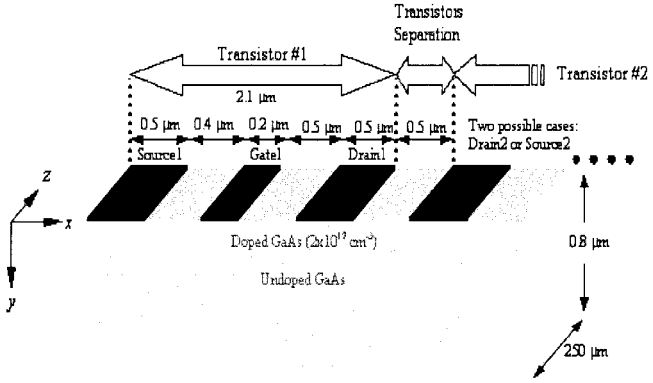

Fig. 10. 3-D view of the simulated transistors (not to scale).

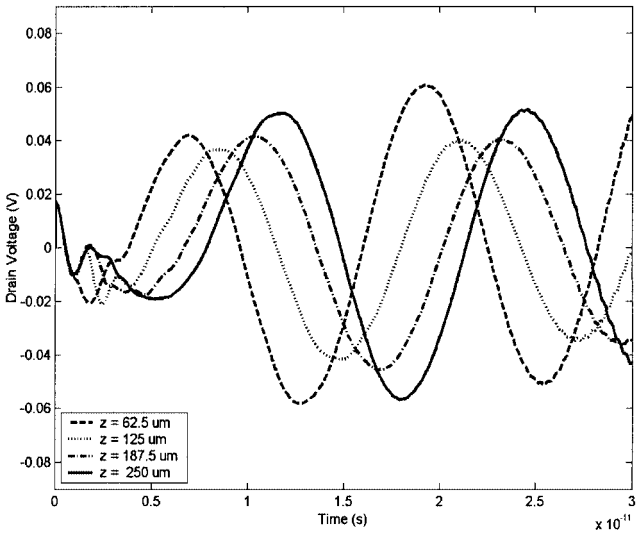

Fig. 11. Drain voltage (normalized) of the simulated transistor when EM-wave propagation and electron-wave interaction are considered at different points in the z-direction.

energy build-up along the device width, and due to the phase-velocity mismatch between the EM waves at the gate and drain electrodes. Fig. 11 demonstrates the importance of coupling the EM waves with the semiconductor transport physics for accurate modeling of millimeter-wave transistors.

Now we turn our attention to the full-wave simulation of the two transistors shown in Fig. 10. First, we assume that one of the transistors is operating, while the other transistor is not. Fig. 12 depicts the simulation results, which emphasize the significance to include the EM-wave propagation effects, not only inside the device, but around it as well. In fact, this is the basic theory of operation of multifinger transistors. Ideally, the nonoperating transistor should have a zero drain voltage; however, due to the proximity of an operating transistor, an induced voltage that varies along the device width is introduced.

Next, the two transistors in the configuration shown in Fig. 10 are simulated, assuming that both transistors are now operating. There are two cases to consider. The first case is to assume the drains of the two transistors are adjacent to each other (the case of multifinger transistors), while the other case is to consider the drain of one of the transistors is adjacent to the source of the other transistor. Figs. 13 and 14 show the simulation results.

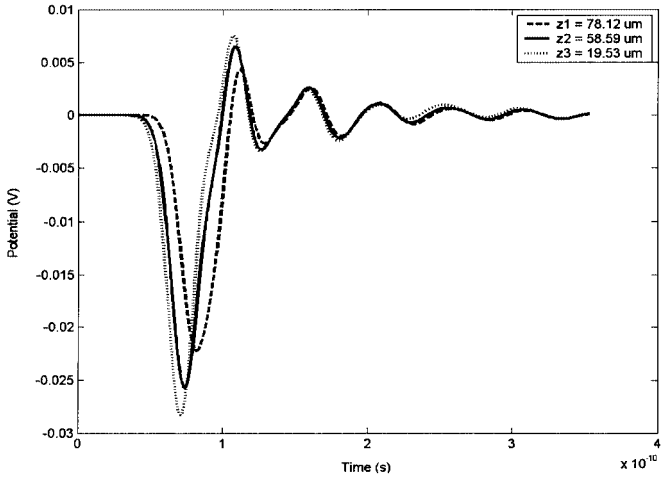

Fig. 12. Potential of a passive electrode at different points in the z-direction induced due to the proximity of an operating transistor excited by a Gaussian signal.

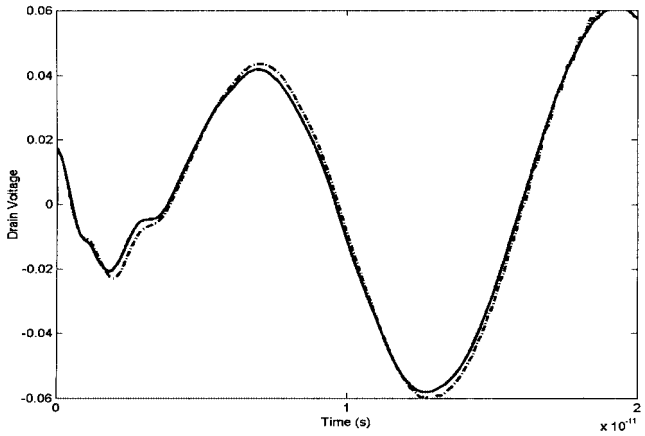

Fig. 13. Drain voltage (normalized) at $z = 62.5$ μm when EM-wave propagation and electron-wave interaction are considered. Solid line: transistor is simulated alone. Dashed line: source electrode of a second operating transistor is 0.5 μm apart from the drain of the simulated transistor.

The first conclusion that can be drawn from the two figures is that the proximity of an operating transistor affects the output voltage due to the EM-wave propagation effects. Furthermore, the EM-wave effects for the case of two adjacent drain electrodes is much larger than the other case. This is expected since the drain electrode has the amplified output signal. It is important to mention that the results in Figs. 11, 13, and 14 are normalized such that the effect of the increase of transconductance with width is not included. The reason is that we are interested only in investigating the effect of EM-wave propagation.

B. EM-Physical Modeling of Multifinger Transistors

It is clear from the previous results that EM-wave propagation and electron-wave interactions change the device characteristics at high frequency. Accordingly, different structure shapes and configurations need to be employed to minimize these effects, aiming to improve the device performance, especially at high operating power and frequency. A possible solution is to use multiple gate fingers of shorter lengths. In this manner,

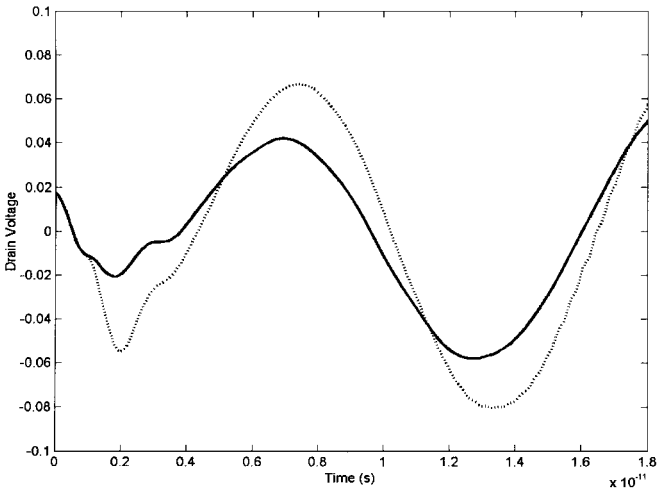

Fig. 14. Drain voltage (normalized) at $z = 62.5$ μm when EM-wave propagation and electron-wave interaction are considered. Solid line: transistor is simulated alone. Dotted line: drain electrode of a second operating transistor is 0.5 μm apart from the drain of the simulated transistor.

EM-wave propagation effects along the device width are minimized. Moreover, attenuation is reduced as a result of reducing the gate metallic resistance. Thus, a large number of fingers is better in terms of reducing attenuation and wave-propagation effects along the device width. However, a large number of fingers means that attenuation and EM-wave propagation effects are increased along the feeding line. Moreover, more fingers may cause more EM-waves interference. Thus, EM-wave synchronization for the multiple fingers is crucial for maximum power and minimum interference. It is noteworthy to state that EM-wave phase-velocity mismatches is due to the different applied voltages to the electrodes and also due to the unsymmetrical shape of the structure. Therefore, the number of fingers and distance between gate fingers should be optimized simultaneously.

Moreover, for the case of the four-finger transistors, the shape and size of the air bridge connecting the different fingers affect the high-frequency characteristics of the transistor. Considering Fig. 15(c), it should be noticed that new capacitances between the air bridge and transistor electrodes $C_{\mathrm{air\_bridge}}$ are created. This would definitely change the EM-wave phase velocities and, as a result, change the device behavior. Thus, an optimal air-bridge structure and size should be employed as well. Furthermore, the air bridge should not be fragile, in order not to break easily, which represents an extra constraint that needs to be included in our optimization problem. The feeding line shape also represents a parameter that needs to be considered for circuit-matching issues.

In this paper, ad-hoc optimization is performed to obtain near-optimal transistor parameters based on the above criteria. Table IV shows the new parameters for the optimized multifinger transistors, and Fig. 15 gives a generic 3-D view of the simulated multifinger transistors.

Output voltages for the simulated multifinger transistors are shown in Fig. 16. Considering this figure, one should observe that the voltage gain increases when using four-finger transistors. In addition, the shape of the output signal for the four-finger

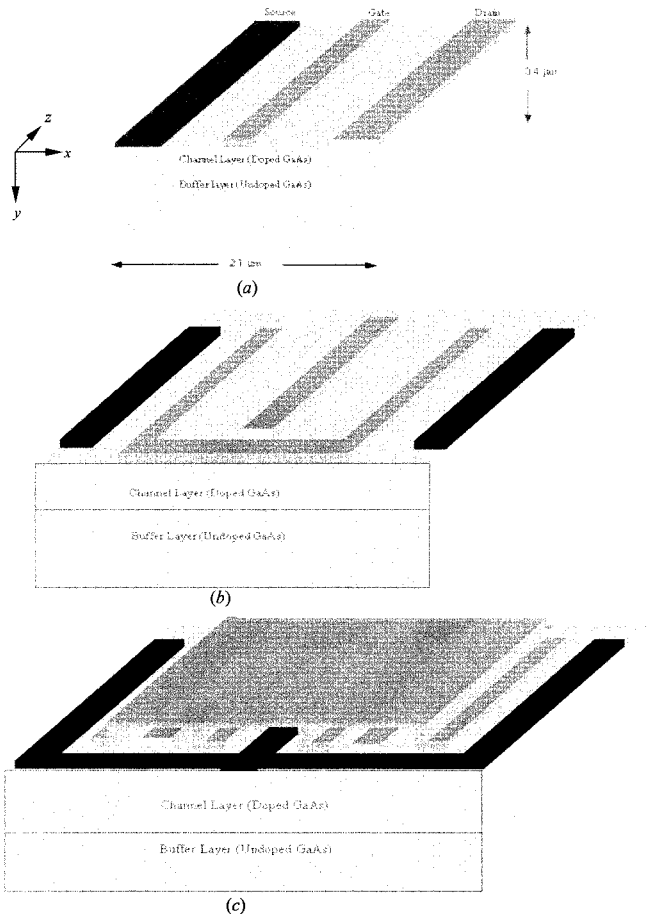

Fig. 15. Generic 3-D view of the simulated multifinger transistors (not to scale). (a) Single-finger transistor ($1 \times 450\ \mu$m). (b) Two-finger transistor ($2 \times 225\ \mu$m). (b) Four-finger transistor ($4 \times 112.5\ \mu$m).

TABLE IV
MULTIFINGER TRANSISTOR OPTIMIZED-PARAMETERS USED IN THE SIMULATION

Drain and source contacts	0.5 μm
Gate-source separation	0.5 μm
Gate-drain separation	0.4 μm
Device thickness	0.4 μm
Device length	2.1 μm
Gate length	0.2 μm
Device Width	1x450, 2x225, 4x112.5 μm
Active layer thickness	0.1 μm
Active layer doping	$2x10^{17}$ cm^{-3}
Schottky barrier height	0.8 V
DC gate-source voltage	-0.2 V
DC drain-source voltage	3.0 V
Operating frequency	60 GHz

transistor case appears to be much better, which means fewer harmonics.

Design and optimization of high-frequency multifinger transistors requires tremendous research. It also requires, as a backbone, a very efficient numerical simulator that includes EM-wave propagation and electron-wave interactions. The simulator should be accurate and, most importantly, fast in order to be suitable for optimizing complex microwave structures. It is our belief that this paper presents this type of simulator.

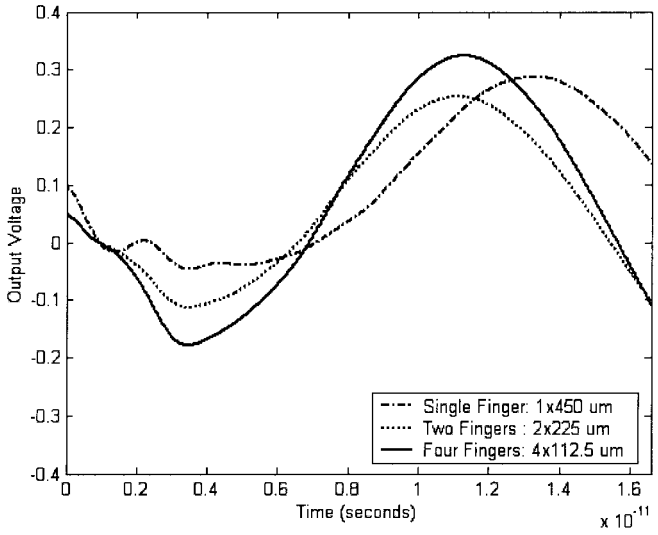

Fig. 16. Output voltage for the simulated multifinger transistors when EM-wave propagation and electron-wave interactions are considered.

This paper also presents, for the first time in literature, the preliminary numerical results of EM physical simulation of multifinger transistors based on ad-hoc optimization. Future research will employ rigorous optimization techniques to obtain the optimal multifinger transistor structure based on the model presented in this paper. Moreover, measurements will be carried out and compared to the results achieved by our model.

IX. CONCLUSION

In this paper, the potential of high-power and high-frequency multifinger transistors has been demonstrated using a new wavelet-based full-wave physical-simulation approach. The proposed technique solves the model that combines the transport physics and Maxwell's equations on nonuniform self-adaptive grids obtained using wavelets. Moreover, efficient grid-updating criteria for the active and passive parts of the problem are developed and verified. A reduction of 75% in CPU time is achieved compared to a uniform grid case with an error of 2% on the dc drain current. In addition, an 80% CPU time reduction is obtained for FDTD simulations with approximately 0.1% average error on the potential. Tradeoffs are observed between the threshold value, CPU time, and accuracy, suggesting an optimal value for the threshold.

The preliminary results of this paper show that, at very high frequency, several phenomena with a strong impact on the device behavior start to emerge, such as phase velocity mismatches, electron-wave interaction, and attenuation. The results suggest that contemporary microwave devices should be optimized to minimize these effects or possibly exploit in favor of improved device characteristics. The results also recommend multifinger transistors as potential alternatives to conventional transistors. This is achieved by using multiple-finger gates of less width instead of a single-gate device. Furthermore, this paper has underlined the enhanced microwave characteristics of multifinger transistors attributable to reducing attenuation and EM-wave propagation effects along the device width. Future research will involve employing rigorous optimization

techniques to obtain the optimal multifinger transistor structure based on the EM-physical model presented in this paper. Moreover, measurements will be carried out and compared to the results achieved by our model.

REFERENCES

[1] A. Garlapati and S. Prasad, "A unified model for single/multifinger HBT's including self-heating effects," *IEEE Trans. Microwave Theory Tech.*, vol. 49, pp. 186–191, Jan. 2001.

[2] M. Snowden, "Large-signal microwave characterization of AlGaAs/GaAs HBT's based on a physics-based electrothermal model," *IEEE Trans. Microwave Theory Tech.*, vol. 45, pp. 58–71, Jan. 1997.

[3] A. Cidronal, G. Leuzzi, G. Manes, and F. Giannini, "Physical/electromagnetic pHEMT modeling," *IEEE Trans. Microwave Theory Tech.*, vol. 51, pp. 830–838, Mar. 2003.

[4] M. Rudolph, R. Doerner, K. Beilenhoff, and P. Heymann, "Scalable GaInP/GaAs HBT large-signal model," *IEEE Trans. Microwave Theory Tech.*, vol. 48, pp. 2370–2376, Dec. 2000.

[5] A. Koudymov, H. Xuhong, K. Simin, G. Simin, M. Ali, J. Yang, and M. A. Khan, "Low-loss high power RF switching using multifinger AlGaN/GaN MOSHFETs," *IEEE Electron Device Lett.*, vol. 43, pp. 449–451, Aug. 2002.

[6] F. Dhondt, J. Barrette, and P. A. Rolland, "Transient analysis of collector current collapse in multifinger HBT's," *IEEE Microwave Guided Wave Lett.*, vol. 8, pp. 272–274, Aug. 1998.

[7] F. Dhondt, J. Barrette, N. Haese, P. A. Rolland, and S. L. Delage, "Finite-element electromagnetic characterization of parasitics in multifinger thermally shunted HBTs," *IEEE Microwave Guided Wave Lett.*, vol. 8, pp. 167–169, Apr. 1998.

[8] L. Chih-Hao and L. Chien-Ping, "Optimum design for a thermally stable multifinger power transistor with temperature-dependent thermal conductivity," *IEEE Trans. Electron Devices*, vol. 49, pp. 909–915, May 2002.

[9] Z. Ma, S. Mohammadi, P. Bhattacharya, L. P. B. Katehi, S. A. Alterovitz, G. E. Ponchak, K. M. Strohm, and J.-F. Luy, "Ku-band (12.6 GHz) SiGe/Si high-power heterojunction bipolar transistors," *Electron. Lett.*, vol. 37, pp. 1140–1142, Aug. 2001.

[10] K. Chang-Woo, N. Goto, and K. Honjo, "Thermal behavior depending on emitter finger and substrate configurations in power heterojunction bipolar transistors," *IEEE Trans. Electron Devices*, vol. 45, pp. 1190–1195, June 1998.

[11] M. Clemens, E. Gjonaj, P. Pinder, and T. Weiland, "Self-consistent simulations of transient heating effects in electrical devices using the finite integration technique," *IEEE Trans. Magn.*, vol. 37, pp. 3375–3379, Sept. 2001.

[12] S. El-Ghazaly and T. Itoh, "Electromagnetic interfacing of semiconductor devices and circuits," in *Proc. IEEE MTT-S Int. Microwave Symp. Dig.*, 1997, pp. 151–154.

[13] S. M. S. Imtiaz and S. M. El-Ghazaly, "Global modeling of millimeter-wave circuits: Electromagnetic simulation of amplifiers," *IEEE Trans. Microwave Theory Tech.*, vol. 45, pp. 2208–2216, Dec. 1997.

[14] A. Witzig, C. Schuster, P. Regeli, and W. Fichtner, "Global modeling of microwave applications by combining the FDTD method and a general semiconductor device and circuit simulator," *IEEE Trans. Microwave Theory Tech.*, vol. 47, pp. 919–928, June 1999.

[15] P. Ciampolini, L. Roselli, G. Stopponi, and R. Sorrentino, "Global modeling strategies for the analysis of high-frequency integrated circuits," *IEEE Trans. Microwave Theory Tech.*, vol. 47, pp. 950–955, June 1999.

[16] M. A. Alsunaidi, S. M. Imtiaz, and S. M. El-Ghazaly, "Electromagnetic wave effects on microwave transistors using a full wave high-frequency time-domain model," *IEEE Trans. Microwave Theory Tech.*, vol. 44, pp. 799–808, June 1996.

[17] R. O. Grondin, S. M. El-Ghazaly, and S. Goodnick, "A review of global modeling of charge transport in semiconductors and full-wave electromagnetics," *IEEE Trans. Microwave Theory Tech.*, vol. 47, pp. 817–829, June 1999.

[18] S. G. Mallat, "A theory for multiresolution signal decomposition: The wavelet representation," *IEEE Trans. Pattern Anal. Mach. Intell.*, vol. 11, pp. 674–693, July 1989.

[19] I. Daubechies, *Ten Lectures on Wavelets*. Philadelphia, PA: SIAM, 1992.

[20] B. McGarvey and E. Tentzeris, "Coupling of solid-state and electromagnetic equations," in *Proc. Eur. Microwave Conf.*, London, U.K., 2001.

[21] E. M. Tentzeris, A. Cangellaris, L. P. B. Katehi, and J. Harvey, "Multiresolution time-domain (MRTD) adaptive schemes using arbitrary resolutions of wavelets," *IEEE Trans. Microwave Theory Tech.*, vol. 50, pp. 501–516, Feb. 2002.

[22] M. Krumpholz and L. P. B. Katehi, "MRTD: New time-domain schemes based on multiresolution analysis," *IEEE Trans. Microwave Theory Tech.*, vol. 44, pp. 555–571, Apr. 1996.

[23] M. Werthen and I. Wolff, "A novel wavelet based time domain simulation approach," *IEEE Microwave Guided Wave Lett.*, vol. 6, pp. 438–440, Dec. 1996.

[24] M. Fujii and W. J. R. Hoefer, "A three-dimensional Haar-wavelet-based multiresolution analysis similar to the FDTD method—Derivation and application," *IEEE Trans. Microwave Theory Tech.*, vol. 46, pp. 2463–2475, Dec. 1998.

[25] S. Grivet-Talocia, "On the accuracy of Haar-based multiresolution time-domain schemes," *IEEE Microwave Guided-Wave Lett.*, vol. 10, pp. 397–399, Oct. 2000.

[26] T. Dogaru and L. Carin, "Scattering analysis by multiresolution time domain method using compactly supported wavelet systems," *IEEE Trans. Microwave Theory Tech.*, vol. 50, pp. 1752–1760, July 2002.

[27] G. Carat *et al.*, "An efficient analysis of planar microwave circuits using a DWT-based Haar MRTD scheme," *IEEE Trans. Microwave Theory Tech.*, vol. 48, pp. 2261–2270, Dec. 2000.

[28] M. Fujii and W. Hoefer, "Field singularity correction in 2-D time-domain Haar-wavelet modeling of waveguide components," *IEEE Trans. Microwave Theory Tech.*, vol. 49, pp. 685–691, Apr. 2001.

[29] T. Dogaru and L. Carin, "Multiresolution time-domain using CDF biorthogonal wavelets," *IEEE Trans. Microwave Theory Tech.*, vol. 49, pp. 902–912, May 2001.

[30] C. Sarris and L. Katehi, "Fundamental gridding-related dispersion effects in multiresolution time-domain schemes," *IEEE Trans. Microwave Theory Tech.*, vol. 49, pp. 2248–2257, Dec. 2001.

[31] M. Fujii and W. Hoefer, "Time-domain wavelet-Galerkin modeling of two-dimensional electrically large dielectric waveguides," *IEEE Trans. Microwave Theory Tech.*, vol. 49, pp. 886–892, May 2001.

[32] J. Keiser, "Wavelet based approach to numerical solution of non-linear partial differential equation," Ph.D. dissertation, Univ. Colorado at Boulder, Boulder, CO, 1995.

[33] M. Holmstron, "Solving hyperbolic PDE's using interpolating wavelets," Uppsala Univ., Uppsala, Sweden, Tech. Rep. 189/1996, 1996.

[34] S. Goasguen and S. M. El-Ghazaly, "Interpolating wavelet scheme toward global modeling of microwave circuits," in *IEEE MTT-S Int. Microwave Symp. Dig.*, 2000, pp. 375–378.

[35] S. Goasguen, M. M. Tomeh, and S. M. El-Ghazaly, "Interpolating wavelet scheme toward global modeling of microwave circuits," in *IEEE MTT-S Int. Microwave Symp. Dig.*, 2001, pp. 415–418.

[36] M. Toupikov, G. Pan, and B. K. Gilbert, "On nonlinear modeling of microwave devices using interpolating wavelets," *IEEE Trans. Microwave Theory Tech.*, vol. 48, pp. 500–509, Apr. 2000.

[37] Y. K. Feng and A. Hints, "Simulation of submicrometer GaAs MESFET's using a full hydrodynamic model," *IEEE Trans. Electron Devices*, vol. 35, pp. 1419–1431, Sept. 1988.

[38] P. Flandrin, *Time-Frequency/Time-Scale Analysis*. San Diego, CA: Academic, 1998.

[39] B. Hubbard, *The World According to Wavelets; The Story of a Mathematical Technique in the Making*. Wellesly, MA: A. K. Peters, 1998.

[40] C. Hilsum, "Simple empirical relationship between mobility and carrier concentrations," *Electron Lett.*, vol. 10, no. 12, pp. 259–260, 1974.

[41] Y. A. Hussein and S. M. El-Ghazaly, "Global modeling of active microwave devices incorporating a novel full hydrodynamic physical simulator using wavelet-based adaptive grids," in *IEEE MTT-S Int. Microwave Symp. Dig.*, 2002, pp. 743–746.

[42] Y. A. Hussein, S. M. El-Ghazaly, and S. M. Goodnick, "A new wavelet-based technique for fast full-wave physical simulations of millimeter-wave transistors," in *IEEE MTT-S Int. Microwave Symp. Dig.*, 2003, pp. 17–20.

[43] Y. A. Hussein and S. M. El-Ghazaly, "Extending multiresolution time-domain (MRTD) to the simulation of high-frequency active devices," *IEEE Trans. Microwave Theory Tech.*, vol. 51, pp. 1842–1851, July 2003.

[44] S. Hammadi and S. El-Ghazaly, "Air-bridged gate MESFET: A new structure to reduce wave propagation effects in high-frequency transistors," *IEEE Trans. Microwave Theory Tech.*, vol. 47, pp. 890–899, June 1999.

Yasser A. Hussein (M'03) was born in Cairo, Egypt. He received the B.S. and M.S. degrees in electrical engineering from Cairo University, Cairo, Egypt, in 1995 and 1998, respectively, and the Ph.D. degree in electrical engineering from Arizona State University, Tempe, in 2003.

He has been with several universities and research centers including Cairo University, the National Institute of Standardization (NIS), Cairo, Egypt, and Arizona State University. He is currently with the Stanford Linear Accelerator Center (SLAC), Stanford University, Menlo Park, CA. His current research interests are in the areas of computer-aided design of microwave integrated circuits, computational electromagnetics and semiconductor high-frequency RF modeling and measurements, and wireless communications.

Dr. Hussein is an elected member of the National Society of Collegiate Scholars and Phi Kappa Phi.

Samir M. El-Ghazaly (S'84–M'86–SM'91–F'01) received the Ph.D. degree in electrical engineering from the University of Texas at Austin, in 1988.

In August 1988, he joined Arizona State University, and became a Professor in 1998. He is currently the Department Head of Electrical and Computer Engineering, University of Tennessee, Knoxville. He has visited and been with several universities and research centers including Cairo University, Cairo, Egypt, the Centre Hyperfrequences et Semiconducteurs, Université de Lille I, Lille, France, the University of Ottawa, Ottawa, ON, Canada, the University of Texas at Austin, NASA's Jet Propulsion Laboratory, Pasadena, CA, CST-Motorola Inc., Tempe, AZ, Institut d'Electronique de Microélectronique et de Nanotechnologie (IEMN), Université de Lille, and the Swiss Federal Research Institute (ETH), Zurich, Switzerland. His research interests include RF and microwave circuits and components, microwave and millimeter-wave semiconductor devices, semiconductor device simulations, ultrashort pulse propagation, microwave-optical interactions, linear and nonlinear modeling of superconductor microwave lines, wave–device interactions, electromagnetics, and numerical techniques applied to monolithic microwave integrated circuits (MMICs).

Dr. El-Ghazaly is a member of Tau Beta Pi, Sigma Xi, and Eta Kappa Nu. He is an elected member of Commissions A and D, URSI. He was the secretary and vice chairman, and is currently the chairman of Commission A, U.S. National Committee of URSI. He is a member of the Technical Program Committee for the IEEE Microwave Theory and Techniques Society (IEEE MTT-S) International Microwave Symposium (IMS) since 1991. He is on the Editorial Board of the IEEE TRANSACTIONS ON MICROWAVE THEORY AND TECHNIQUES. He was the chairman of the IEEE Waves and Devices Group, Phoenix Section. He was the chapter funding coordinator and chairman of the Chapter Activities Committee of the IEEE MTT-S. He is an elected member of the Administrative Committee of the IEEE MTT-S. He is the editor-in-chief of the IEEE MICROWAVE AND WIRELESS COMPONENTS LETTERS. He was the general chairman of the IEEE MTT-S 2001 IMS, Phoenix, AZ, May 2001.

Stephen M. Goodnick (M'87–SM'92) received the B.S. degree in engineering science from Trinity University, San Antonio, TX, in 1977, and the M.S. and Ph.D. degrees in electrical engineering from Colorado State University, Fort Collins, in 1979 and 1983 respectively.

He was an Alexander von Humboldt Fellow with the Technical University of Munich, Munich, Germany, and the University of Modena, Modena, Italy, in 1985 and 1986, respectively. From 1986 to 1997, he was a faculty member with the Department of Electrical and Computer Engineering, Oregon State University, Corvallis. He is currently the Chair and a Professor of the Department of Electrical Engineering, Arizona State University, Tempe. He has coauthored over 130 journal papers, books, and book chapters related to transport in semiconductor devices and microstructures.